Entropy frameworks for urban heat storage can support targeted adaptation strategies

Daniel Hertel, Uwe Schlink*

Helmholtz Centre for Environmental Research – UFZ, Department of Urban and Environmental Sociology, Permoserstraße 15, 04318, Leipzig, Germany

KEYWORDS: urban climate modelling, ENVI-met, heat storage hysteresis, urban climate adaptation, entropy

ABSTRACT: The attribution of urban temperatures to biophysical processes (*Zhao et al., 2014; Ridgen & Li, 2017, Li et al, 2019*) improves the understanding of the urban heat island (UHI) phenomenon. Traditionally UHI studies are based on satellite observations, which are limited in their spatial resolution. Little is known about how the biophysical contributions are composed at micro-scale (some meters) and how they interact. Here we suggest an entropy concept for the heat storage cycle, reducing the complexity of the system and improving the understanding of hysteresis. The entropy framework was applied to different surface types based on micrometeorological simulations (3 m × 3 m horizontal resolution) that are validated by an airborne thermal scan. In addition to the effects of reduced convection and evapotranspiration we found that heat storage can make a very dominant contribution locally. It proceeds in entropy loops, where steep slopes and maximally symmetrically closed loop areas are optimal for achieving a balance between heat storage and release. The characteristics of the entropy cycles help suggest new and optimised strategies to attenuate urban heat episodes and we present a stepwise procedure (workflow) for the application of this method.

*Corresponding author. Tel.: +49 341 235 1704; Fax: +49 341 235 45 1704
Email address: daniel.hertel@ufz.de

1. INTRODUCTION

Cities unite a significant part of world's population and, thus, play an increasing role for the impacts of global climate change. Creating their own climate (*Kalnay, 2003*), cities are strongly dominated by local effects but affect larger scales by material transfer over the boundaries because of their open system characteristics. Currently, there are efforts in upscaling urban information/data for global climate solutions (*Creutzig et al., 2019*) and harmonizing global urban data (*World Urban Database and Access Portal Tools - WUDAPT*). Upscaling requires detailed knowledge about local processes such as the urban heat island (UHI) effect which measures the urban-rural temperature difference (ΔT). While nocturnal UHI is largest for air temperatures (associated with city's population size (*Oke, 1973; Zhao, 2014*), the daytime UHI is most pronounced for the surface temperatures which depend on the energy balance that is driven by five biophysical processes: (i) trapping of radiation, (ii) reduced evapotranspirative cooling, (iii) reduced convection, (iv) heat storage in urban materials, and (v) release of anthropogenic heat. A quantification of these five UHI contributions is desirable for the implementation of efficient heat adaptation measures (*Hertel & Schlink, 2019a*). In light of the increasing persistence and frequency of heat waves after 1997 (*Christidis et al., 2015; Morabito et al., 2017*), city authorities face the challenge of combining an optimal mixture between technical solutions and cost-benefit considerations with regard to the very heterogeneous UHI ('archipelago' structure (*Kuttler, 2012*)). Urban surfaces are composed of a variety of different surface types, green infrastructures and building materials which affect the surface energy balance so that considering only selected points is just as inadequate as the use of coarsely resolved satellite images for the development of local heat adaptation strategies.

Complementing most UHI studies that investigate just the amount of ΔT, here we analyse the dynamics that are particularly interesting for heat storage, which has a characteristic hysteresis (*Camuffo & Bernardi, 1982*) effect combined with net radiation. The daily cycle of irradiance forms a closed loop which is caused by a shift between the daily maxima of heat storage flux and surface temperature. A first physical explanation for the hysteresis loop was given by *Grimmond et al. (1991):* "In the morning, before the nightly inversion layer disappears, the atmosphere is mostly stable and the mixing layer very narrow with a low vertical thickness. This allows for an easy transport of sensible heat downwards to the surface. Then, in the afternoon, the atmosphere is mostly unstable stratified and the coupling between boundary layer and surface layer is greatest.

In this way, turbulent transport into the atmosphere dominates and the heat conduction into the soil becomes inefficient." *Sun et al.* (2013) explained the hysteresis by a phase shift between heat storage and net radiation that depends on different surface materials. Later on they additionally included liquid water transport and enhanced the application of Grimmond's hysteresis parameterisation (Objective Hysteresis Model – OHM, *Grimmond et al., 1991*) by an improved physical interpretation of the OHM coefficients (*Sun et al., 2017*). An application of this hysteresis concept to urban heat adaptation is still missing which makes it difficult for policy makers to guide appropriate measures, in particular for heat storage reduction.

Since heat storage changes and interacts with the other biophysical factors throughout the day, we need to describe a very complex system that, nowadays, can be predicted by advanced data science techniques (machine learning), such as deep neural network (DNN) architectures (*Oh et al., 2020*). Such methods have the disadvantage that it is often extremely difficult to determine how the model achieves the predicted results ("black box" problem; *Zednik, 2019*). Entropy is a metric that characterizes such a complex system but allows for better interpretation of the underlying processes than, e.g. current DNN architectures where Shannon entropy is used as a measure of uncertainty. In a statistical entropy interpretation, the urban climate represents an open thermodynamic system where the most likely scenario is the maximum entropy state (further explanations for the entropy maximisation principle can be found in *Purvis et al., 2019*). However, here, in this study, we apply a different entropy concept to the storage of heat in urban surfaces (e.g. buildings, pavement materials, and ground). This demonstrates how such insights can help to optimise and support a more targeted design of local mitigation and adaptation measures to urban climate change, aiming at locations where heat storage plays the dominant role (*Hertel & Schlink, 2019a*). By means of this concept we suggest a new explanation of the previously described hysteresis (*Grimmond et al., 1991*) between net radiation and heat storage.

For thermodynamic systems with heat exchange, the entropy *dS* is defined as

$$dS = \frac{\delta Q}{T}, \tag{1}$$

where T is the temperature and δQ the heat intake into the system. In the 19th century (*Clausius, 1865*), the entropy concept evolved from describing thermodynamic cycles and was used to assess the amount of energy that is transformed in terms of usable work. Typical examples are heat engines or heat pumps that convert between thermal and mechanical energy. They increase the entropy of the system for an irreversible process and maintain it for reversible ones. Other examples are open atmospheric systems which need negative entropy fluxes (e.g. severe synoptic-scale storms (*Liu & Liu, 2004*)) in order to maintain their ordered structure. When this flux weakens or turns positive then they lose their structure and dissipate. Although the mentioned examples involve gaseous mediums, the entropy definition can be transferred to other aggregate states. For instance, *Singh* (2010) suggested an entropy theory for the vertical movement of moisture in unsaturated soils.

While previous UHI studies mainly considered the impact of evapotranspiration and convection on urban heat (*Zhao et al., 2014; Ridgen & Li, 2017; Li et al., 2019*), here we focus on the role of heat storage in urban surfaces and establish an entropy concept as a useful tool for the decision-making process behind impactful and tailor-made adaptation solutions. Our study aims to

(1) discuss urban heat storage as a daily change in entropy for different surface types and apply this new metric to the formation of hysteresis loops,

(2) give a location-independent framework of how to optimise heat storage and release for the purpose of urban adaptation to climate change and a more targeted urban climate management.

2. MATERIALS AND METHODS

2.1 Entropy concept for urban heat storage. The conversion of (short and long-wave) radiation to heat leads to entropy production at the urban surfaces (*Brunsell et al., 2011*) and the following storage of heat in the urban ground is associated with a change in the local entropy. Following eq. 1 the change in entropy ΔS_t (in J K m^{-2}) at time t (each full hour, according to ENVI-met output) for each defined surface type, is calculated by

$$\Delta S_t = -\frac{Q_t}{T_{t,sfc}}, \qquad (2)$$

with $T_{t,sfc}$ = surface temperature and Q_t = ground heat flux in W m^{-2}. The continuous ground heat flux Q(t) can be determined from the spatial derivative of soil temperature at the surface boundary $\left(Q(t) = \frac{\partial u(x,t)}{\partial x} \Big|_{x=0};\ \text{u is soil temperature (see 2.4)}\right)$. In our study, the entropy was calculated by two different methods: First, for eq. 2, the ground heat flux and surface temperatures were extracted from ENVI-met simulations (2.2) and hourly averaged over the respective surface type. Second, an easily interpretable toy model for the conduction and storage of heat in the ground (see 2.4) was used for entropy calculation. Both results are compared by means of a T-S diagram (see 3.1).

2.2 Micrometeorological simulations and partitioning of temperatures. The 3D micrometeorological model ENVI-met v4.4 (*Bruse & Fleer, 1998*), served as simulation tool using meteorological input variables (see Table S1 in Supplementary) and simulating an 'urban state' (current urban structure) as well as a 'rural state' (all buildings and sealed surfaces were replaced by grass) for the neighbourhood 'Bayerischer Bahnhof' in Leipzig (Germany) on September 23rd, 2010. The model was forced with daily cycles of air temperature and relative humidity (data are provided by the nearby Leipzig Institute for Meteorology). For each pixel (size 3 × 3 m) the UHI intensity ($\Delta T = T_{urban} - \overline{T_{rural}}$) was calculated as difference between temperatures simulated for the 'urban' and (mean) 'rural' states while the ground heat flux was directly extracted from ENVI-met output.

Applying the UHI partitioning procedure described in *Hertel & Schlink (2019a, b)*, we derived the contributions to ΔT due to radiation, convection, evapotranspiration, and heat storage (ΔT_{stor}). Each of these parts of ΔT was considered for different surface types (median values for asphalt (mainly streets and parking lots), sand, yellow bricks (streets and pavements), red bricks (streets and pavements), concrete pavement, loam, bare soil, loam with grass, loam with trees (subtypes for different heights and crown leaf area densities), loam with hedge; see Table S2 and Fig. S1 in Supplementary). Vegetation is always combined with a loamy soil which is why these are composites of two types. 'Loam' means all surfaces (except built-up structures) with loam **and/or** vegetation. 'Bare soil' encompasses only loamy soils without any built-up structure or vegetation.

2.3 Thermal scanning. After sunset, on September 22nd evening (19:30 – 21:00), the city of Leipzig was scanned with a thermal camera (for compatibility the ENVI-met simulations, section 2.2, had been performed for the same days) and was used for a validation of the simulated surface temperatures (see Fig. S2 with some explanations).

Using ArcGIS, bilinear resampling was applied (image resolution 5 × 5 m changed to ENVI-met grid of resolution 3 × 3 m) and the study area 'Bayerischer Bahnhof' was extracted by geo-referencing the model output (including a rotation of the simulated area and removal of 2 rows and columns of edge-pixels). The 256 grey levels registered by the camera were calibrated by means of a regression fit to 10 fixed ground stations (*Schlink et al., 2014*).

2.4 Simplified model for urban heat storage. Surface temperatures follow a daily cycle according to the absorbed solar radiation. The gradient between ground and surface temperature determines the strength and direction of ground heat flux so that the vertical propagation of heat within the soil-surface system follows a cyclic function that converges at some depth.

With soil depth $x \in [0, \infty)$, the ground represents a semi-infinite medium with the surface as upper boundary ($x = 0$). A simplified heat conduction problem is:

1D heat equation: $$\frac{\partial u(x,t)}{\partial t} - D\frac{\partial^2 u(x,t)}{\partial x^2} = 0, \ \ \{x > 0, t > 0\} \quad (3)$$

Initial condition (IC): $u(x,0) = 0$

Boundary condition (BC): $u(0,t) = f(t) = \ T_0 - T_1 \cos(\omega t)$

Decay condition: $u(x,t) \rightarrow T_0 \ \ for\ x \rightarrow \infty\ and\ t \rightarrow 0,$

where $u(x, t)$ is the temperature at soil depth x and time t (in h), T_0 and T_1 are mean and amplitude, D is the thermal diffusivity (in $m^2\ s^{-1}$) and $\omega = 2\pi/24h$ is the angular frequency of one day.
The steady state solution for the problem (eq. 3; for a detailed derivation of the solution see supplementary) is given by,

$$u(x,t) = T_0 - T_1 e^{-\sqrt{\frac{\pi}{Dt^*}}x} \cos\left(-\sqrt{\frac{\pi}{Dt^*}}x + \frac{2\pi}{t^*}t\right). \quad (4)$$

$t^* = 24 \times 3600$ s is a characteristic time while t is variable ({0, 24, 1h}). x represents the soil depth and x/x^* is a dimensionless form (Fig. 1, see supplementary for x^*). For $x \rightarrow \infty$, the exponential function in eq. 4 is 0 resulting in $u(x, t) = T_0$. At this depth, the daily temperature cycle decays (Fig. 1). For $x = 0$, eq. 4 represents the development of the daily surface temperature, and the ground heat flux at the surface can be derived (see eq. 5).

Fig.1 reveals that, for sealed surfaces, the propagation of heat can spread to deeper soil layers than for vegetated surfaces. Because of the shading effect through vegetation also the temperature variance throughout the day is considerable smaller. While for vegetated surfaces $u(x, t) = T_0$ after around 25% of the total soil depth, for sealed surfaces this is achieved after approx. 30-35%.

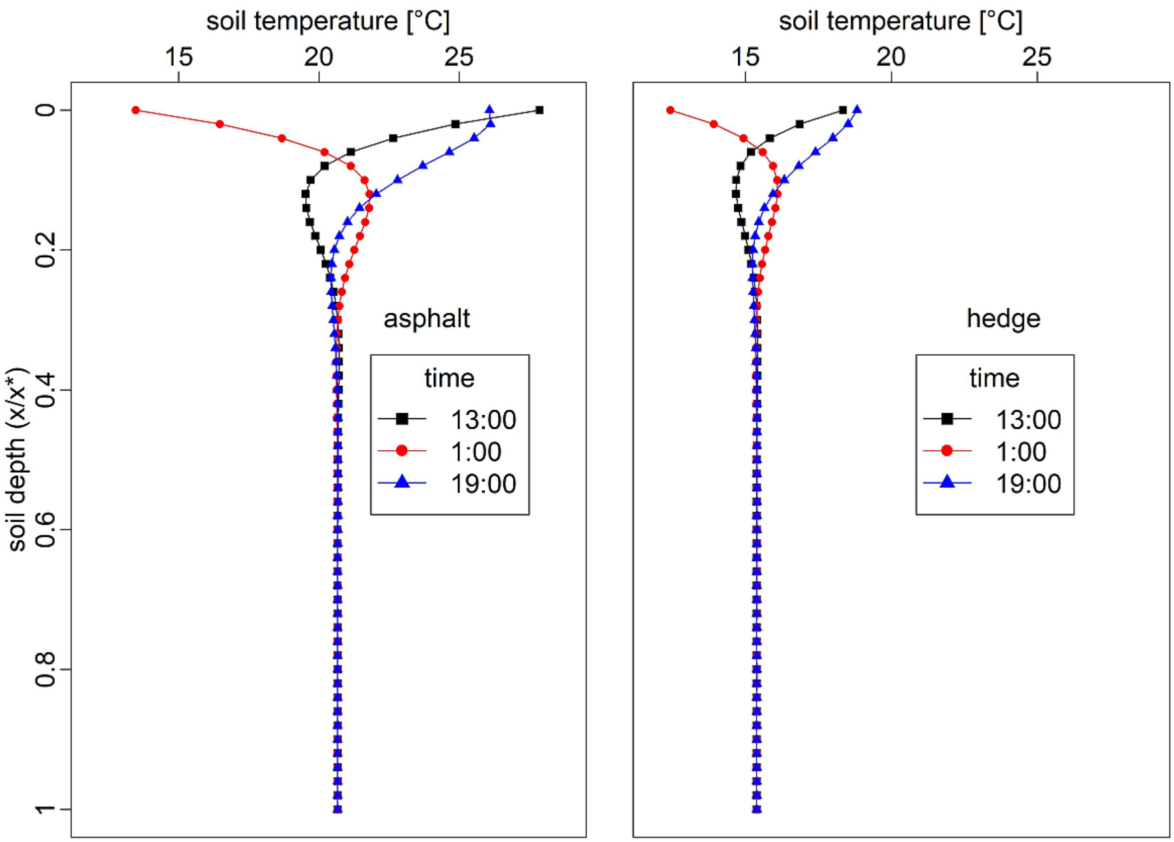

Figure 1. Soil temperature for different times dependent on depth. Soil depth is dimensionless (x/x*; 0 = surface). Left graph is typical for sealed surfaces (example: asphalt) and right graph for vegetated surfaces (example: hedge).

The ground heat flux at the surface is

$$Q(t) = -\lambda \frac{\partial u(x,t)}{\partial x}\Big|_{x=0} = -\lambda \times T_1 \times \sqrt{\frac{\pi}{Dt^*}}\left(\cos\left(\frac{2\pi}{t^*}t-\psi\right)-\sin\left(\frac{2\pi}{t^*}t-\psi\right)\right). \quad (5)$$

λ (in W $m^{-1} \cdot K^{-1}$)) is the thermal conductivity of the surface material. ψ is an additional phase shift that was introduced to take into account the typical temporal delay between Q_t and $T_{t,sfc}$ which was found by *Lettau (1951)*.

With eqs. 4 and 5 the change in entropy results in

$$\Delta S_{t,model} = -\frac{Q(t)}{u(x=0,t)}. \quad (6)$$

For each surface type, the parameters T_1, ψ, and λ are estimated from an optimal fit of the data to the ENVI-met output (constrained optimisation using PORT routines with quasi-Newton optimizer; nlminb method in R). In order to guarantee that the enclosed area of the respective Q –

T plots (from ENVI-met and our simplified model) are equal, we used a Lagrange multiplier during the optimisation procedure. Furthermore, we added an additional time independent Q_0 to eq. 5 assuring that the ground heat flux cycle has the same starting point as provided from the ENVI-met data; Q_0 was also estimated during the optimisation.

3. RESULTS

3.1 Heat storage in urban surfaces. The diurnal radiation, cyclically heating the surface, generates a periodic change in surface entropy (see 2.4). This is represented by an anti-clockwise ellipsis in the T-S diagram. The grey (α) and thick coloured line (β) in Fig. 2a&b denote the entropy ($\Delta S_{t,model}$) that was calculated from the heat conduction toy model (explained in supplementary). The thin coloured line and points (Fig. 2a&b, γ) represent the entropy (ΔS_t) that was derived from ENVI-met simulations. The change in entropy was calculated for each surface type (definition in 'Material and Methods' section) as an average value over all grid cells for the respective surface type. During daytime (grey line (α), between 6:00 and 17:00, right from the red dotted vertical line representing $\Delta S = 0$), the entropy $\Delta S_{t,model}$ is positive (i.e. from surface into ground), and negative during nighttime. Eq. 2 (see 'Materials and Methods') shows that the direction of the change in entropy depends on the orientation of the ground heat flux. The elliptic form of the loop as well as the vanishing entropy budget refer to the idealised model for heat conduction into ground (section 2.4).

In contrast, for the ΔS_t the loop is not symmetric, which implies that the heat conducted into ground is subsequently not released in the same amount, but rather stored and dissipated inside deeper soil layers (for $\Delta S_t > 0$). Following this finding, we added a constant heat flux to the derived ground heat flux at the surface (eq. 5) and estimated it together with the other parameters in an optimisation procedure (section 2.4). The additional heat flux shifts the ellipsis for the idealised model ($\Delta S_{t,model}$) more to positive values and improved the agreement with ΔS_t.

Ground heat flux (Q_t) and surface temperature ($T_{t,sfc}$) have a time shift of ≈2 – 3 h. Eq. 2 connects both to the entropy so that also entropy and surface temperature inherit a phase shift. In the morning, the daily cycle of ΔS_t is driven by increasing radiation. In the afternoon the heat transport into the soil becomes inefficient due to enhanced turbulent vertical transport (*Grimmond et al., 1991*). As a result, surface temperature drops, but with a delay between surface temperature decrease and heat transport from soil to surface (Fig. S4).

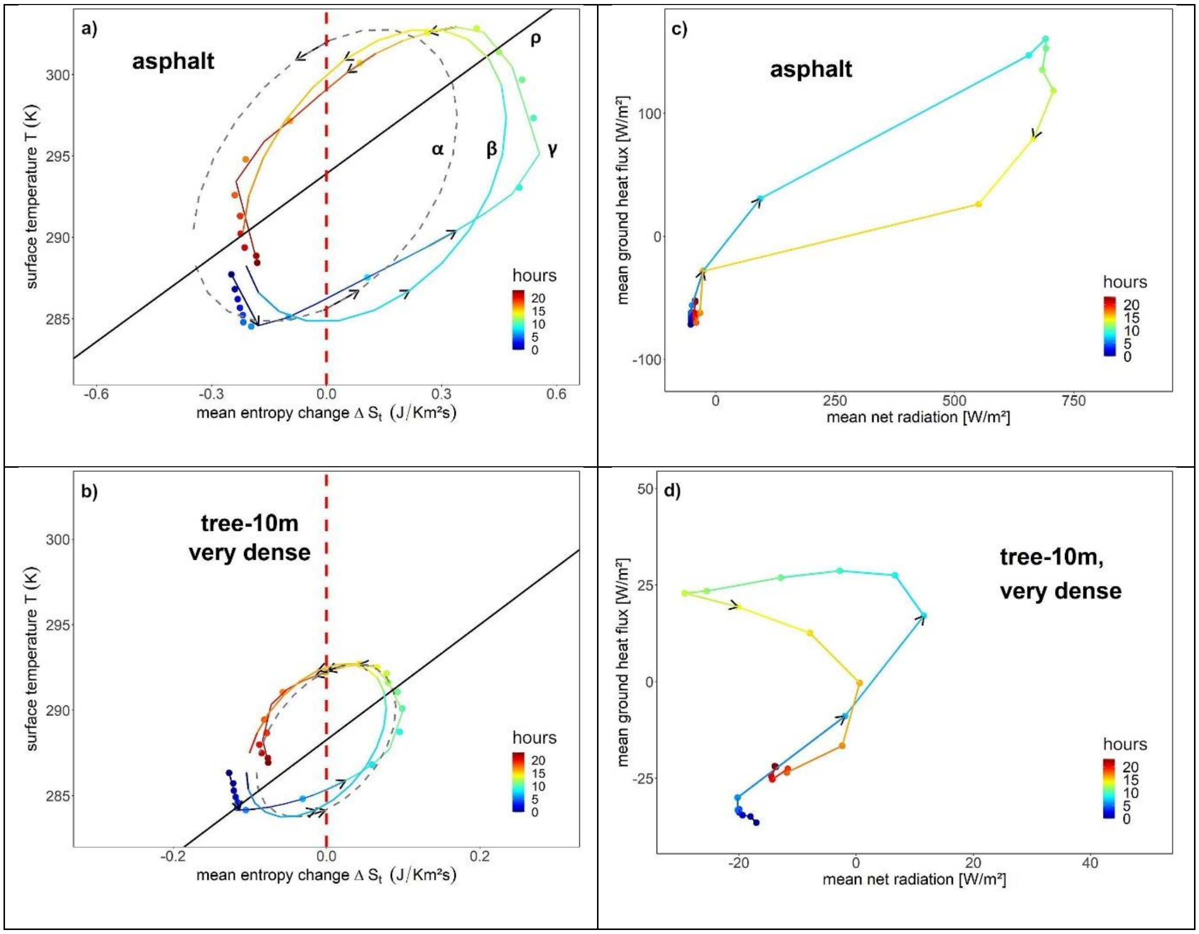

Figure 2. Change in entropy (J K^{-1} m^{-2} s^{-1}) versus mean surface temperature (K) for **(a)** asphalt (top left) and **(b)** loam with tree (bottom left). Mean ground heat flux (W m^{-2}) dependent on mean net radiation (W m^{-2}) per hour of the day for **(c)** asphalt (top right) and **(d)** loam with tree (bottom right). The ellipses represent a fitted ideal heat conduction model ($\Delta S_{t,model}$; **(α)** grey dashed without additional heat flux; **(β)** thick coloured line with adding a constant heat flux), **(γ)** the thin coloured line (ΔS_t) is a cubic smoothing spline (exact method after *Forsythe, Malcolm and Moler (1977)*) fitted to ENVI-met simulations represented by the coloured points around the spline. All Figs. are made for September 23rd, 2010 commencing at 0:00; colours represent time (in h). Arrows denote the looping direction. The red dashed vertical line (ΔS_t = 0) separates between upward and downward change in entropy. The diagonal black line **(ρ)** is a linear regression line indicating the slope of the ΔS_t loop (for all surface types see Figs. S3 (entropy) and S6 (hysteresis) in Supplementary).

A consequence of the loop between entropy and surface temperature (Fig. 2a&b) is a phase shift between radiation intensity and heat storage, resulting in a hysteresis (*Camuffo & Bernardi, 1982*; Fig. 2c&d, see also Fig. S6). For ‘loam with tree’ (Fig. 2d), the hysteresis has a counterclockwise orientation, for asphalt a clockwise orientation. Drier soils result in a clockwise loop, wetter soils in the opposite (*Sun et al., 2013*; humid soils have higher thermal conductivity *(Roxy et al., 2014)*). The typical volumetric water content at 2 p.m. (September 23rd 2010), as calculated within ENVI-met for the 3 high vegetation types (see last 3 rows in Table 1 or S2), is 0.11 – 0.16 m^3 m^{-3} while for the other ≈0.0 – 0.05 m^3 m^{-3}.

The intersection (Fig.2d) is a result of land use interactions and their properties. For instance, in case of vegetation, the plant leaves re-emit the absorbed radiation as long-wave radiation on their lower side to the ground and increase the net surface radiation balance although sun level sinks in the afternoon. In general, since hysteresis is driven by the daily radiation cycle the orientation of the defined surface types against solar radiation and their surface coverage is more important than the heat capacity of each surface material.

3.2 Properties of entropy loops.

Entropy loops can be idealised as ellipses that have two distinct properties: slope (similar to the a_1 coefficient in the OHM *(Grimmond et al., 1991; Oke et al., 2017*) and representing the phase shift leading to a delayed or immediate warming of the surface type) and size of the enclosed loop area (representing the amount of energy transferred during the daily heat storage cycle). While the slope was derived from a linear regression line between the vertexes of the ellipse (black line in Fig. 2), the size of the enclosed loop area was determined by help of a numerical integration procedure (trapezoidal method).

Entropy loops calculated for all different surface types (Fig. S3) cluster into 4 groups (red, light yellow, dark yellow and green dots in Fig. 3). One can distinguish between the groups in terms of overarching surface classes like ‘sealed’ or ‘unsealed’. It turned out that for open land, grass and sand define a separate group. The red group encompasses all sealed surfaces (asphalt, brick-yellow, brick-red, and concrete). Their enclosed loop area sizes vary between ≈5.5 – 9 W m^{-2} d^{-1} and are by far the largest, but the slopes are the most shallow (≈ 13.3 – 17.2 K^2 m^2 W^{-1}). It can be concluded that the surface temperature decreases less with increasing ΔS_t and vice versa compared to the other groups. As a result more heat is stored and transformed during the loop which in turn ends up with larger enclosed loop area size but not necessarily to a positive heat storage contribution to UHI (see section 4 for a discussion).

The yellow and green groups represent ‘unsealed’ surfaces. The dark yellow group consists of sand and grass with an enclosed loop size of ≈2.3 – 2.5 W m^{-2} d^{-1} and has steepest slopes (≈ 46.7 – 49.9 K^2 m^2 W^{-1}). Grass insulates the surface (for example, thermal conductivity amounts to $\lambda \approx$ 0.04 W $m^{-1}\cdot K^{-1}$) for grass processed as insulation material and to 0.14 – 0.21 W $m^{-1}\cdot K^{-1}$ for the underlying soil of grass on a green roof (*Capozzoli et al., 2013*)), so that heat cannot deeply penetrate into the underlying material. This behaviour is similar to (dry) sand ($\lambda \approx$ 0.15 – 0.27 W $m^{-1}\cdot K^{-1}$); *Hamdhan & Clarke, 2010*) while, e.g., heat conduction into pavement is much stronger ($\lambda \approx$ 0.8 – 2 W $m^{-1}\cdot K^{-1}$); *U.S. Department of Transportation, 2020*).

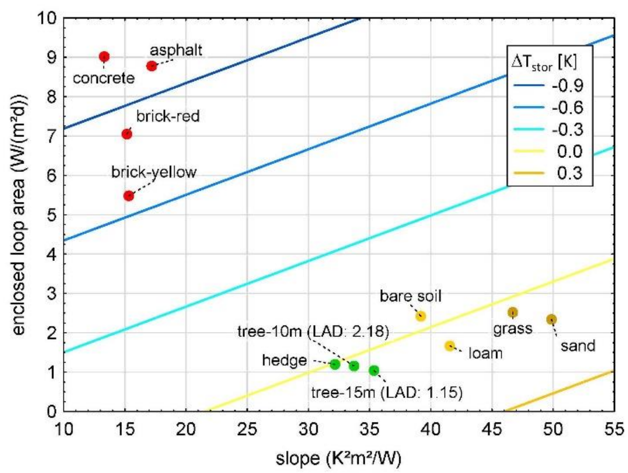

Figure 3. Properties (slope and enclosed loop area) of the entropy loop ΔS_t for the surface types cluster in 4 groups (red = sealed surfaces, green = unsealed with high vegetation, light yellow = unsealed for open land and loam, dark yellow = grass + sand); LAD = leaf area density. Coloured lines represent linear interpolations of the UHI contributions from heat storage (ΔT_{stor}) at the daily maximum (11:00).

For the light yellow group (loam and bare soil) there is no insulation effect like grass which shifts them more to the high vegetation group. Consequently, the slope of the ellipsis is lesser (39.2 – 41.7 K^2 m^2 W^{-1}) than that of grass but larger than that of high vegetation. Eventually, the green group includes all 3 highly vegetated surface types (loam with tree and loam with hedge; see last 3 types in Table 1) which show the smallest enclosed loop area sizes according to their higher cooling potential.

Table 1. Properties (slope and size of the enclosed loop area) for $\Delta S_{t,\,model}$ and ΔS_t in Fig. 3

surface types	area size [W m^{-2} d^{-1}] $\Delta S_{t,model}$	area size [W m^{-2} d^{-1}] ΔS_t	area size [W m^{-2} d^{-1}] ΔS_t day	area size [W m^{-2} d^{-1}] ΔS_t night	slope [K^{2}m^2 W^{-1}]
asphalt	8.794	8.78	6.295	2.485	17.21
brick-yellow	5.476	5.476	3.79	1.686	15.32
brick-red	7.054	7.047	5.169	1.877	15.17
concrete pavement	9.011	9.015	6.207	2.808	13.332
loam	1.661	1.669	0.886	0.782	41.569
bare soil	2.411	2.423	1.169	1.254	39.187
sand	2.342	2.337	1.489	0.848	49.866
loam with grass	2.525	2.518	1.657	0.862	46.702
loam with tree (10 m, LAD: 2.18)	1.147	1.154	0.528	0.626	33.737
loam with tree (15 m, LAD: 1.15)	1.035	1.042	0.437	0.605	35.360
loam with hedge	1.185	1.195	0.543	0.651	32.169

The slopes are not steepest since the entropy range is smallest (≈ -0.1 – 0.1 J K^{-1} m^{-2} s^{-1}) so that the change in surface temperature is also smaller compared to the other groups because of stronger shadowing under dense vegetation canopies. This effect and the air volume between crown and surface increases the phase shift between surface temperature and ground heat flux compared to the yellow groups flattening the slope. Thus, it means that for the high vegetation surface types a delayed warming takes place and heat can conduct into deeper soil layers than for, e.g., sand or bare soil where steeper slopes allow for faster surface warming but also cooling. On the one hand, a delayed warming allows for more heat storage but on the other hand, as mentioned above, the enclosed loop area size is smallest leading to lowest daily amount of transferred energy. In total, the combined effects of both the daily dynamics in heat conduction (slope) and energy transfer (enclosed loop area size) compensate each other so that daily heat storage is small.

The UHI contribution from heat storage (ΔT_{stor}, see section 2.2) at 11:00 shows a clear gradient (coloured lines in Fig. 3) from cooling (red group) to warming (green and dark yellow group) which highlights the influence of the respective surface type on the local UHI. Sealed surfaces show negative values because during day the ground heat flux is directed into soil which transports heat away from the surface. This results in a cooling effect relative to the rural situation although the surface can be very hot through absorption of shortwave radiation. For unsealed surfaces this effect is less pronounced or even reversed. During night the ΔT_{stor} gradient in Fig. 3 is reversed and, consequently, the sealed surfaces provide warming. It should be noted that in our case (study area 'Bayerischer Bahnhof') most sealed surfaces are within residential areas where buildings provide a lot of shading. This strengthens the cooling effect during day. It is clear that the local built-up structure has a massive impact on these results and can be different in other neighbourhoods or cities. In result, from Fig. 3 one can directly read off the UHI contribution of an arbitrary surface (given that it was simulated by the presented approach).

4. DISCUSSION

In the present study, we established an entropy concept as a new location-independent approach for the local abatement of urban heat storage and explained the hysteresis effect for different surface types. Although the urban-rural heat storage difference is composed of variations in thermal properties, moisture availability and geometric form (*Oke et al., 2017*), the hysteresis is a result of these interactions and can be captured via our suggested entropy concept.

In daytime, the ground absorbs incident radiation and the surface heats up. Thus, a vertical temperature gradient between surface and deeper soil layers evolves, enabling a ground heat flux that transfers heat into ground. During night, radiative surface cooling leads to a heat transfer from ground to surface. Since the change in surface temperature is delayed against the ground heat flux, a loop can be observed (see Q-T diagram in Fig. S5). Daily heat conduction and propagation into ground can be approximated by a toy model (see 'Materials and Methods').

The area enclosed by an entropy loop (Fig. 2a&b) is the, via heat storage, consumed daily energy amount per m² and day on the respective surface taken from the incoming solar radiation. For an ideal symmetric entropy loop there is no gain or loss – positive and negative areas compensate each other. Heat storage in the ground shows a similar thermodynamic behaviour as a heat pump (both describe an anti-clockwise loop in the T-S-diagram) and the external energy intake is provided by the solar radiation cycle. In a mechanical heat pump system (e.g. refrigerator) a compressor provides heat transport from a cold reservoir to a hot reservoir by help of energy supply (enclosed loop area is consumed mechanical work).

The ground heat storage system has a different mechanism: During light day, the ground itself is a ‘cool reservoir’ and the illuminated surface becomes a ‘hot reservoir’: heat flux is directed into the ground. With sunset the solar radiation input decays. During nighttime, long-wave emissions cool the surface down and transform it from a hot to a cold reservoir. Now, ground temperatures exceed surface temperatures and the heat flux is reversed from ground to surface. The change of the thermodynamic state is not mechanically induced through an expansion or compression, but rather because of radiative heating/cooling. The state variable entropy is proportional to the daily transformation cycle between high-energy (low entropy) and low-energy (high entropy; *Kuricheva et al., 2017*). This means, during the day, the system dissipates more heat into the soil while in the afternoon or during night the lower entropy near the surface enables heat release (“entropy pump” driven by irreversible processes within the soil; *Fortak, 1979*). Photons of the absorbed short-wave radiation (day) contain lower entropy than the emitted long-wave radiation (night; *Wu & Liu, 2010*). Therefore, during day the entropy near the soil surface is low (entropy flow directed to surface) and during night high (entropy flow directed into soil).

The larger the area of the loop, the more heat is transferred between the hot and cold reservoirs during a daily cycle. This does not necessarily mean that the respective heat storage contribution to UHI (Fig. 3) provides stronger warming: the more heat is transferred from the surface to the ground, the stronger is the relative cooling effect compared to a rural situation. It also depends on the amount of heat that is released during night. Fig. 3 is plotted for only one point in time (11:00), but the entropy loops represent daily cycles which might lead to different UHI contributions throughout the day. Therefore, in our example at 11:00 (Fig. 3), for the purpose of targeted and effective climate adaptation measures, the enclosed loop area should be maximised to minimise the heat storage contribution to UHI, and avoid a positive temperature trend over several days.

The slope of an entropy loop (Fig. 2a&b) is the phase shift between temperature and entropy indicating whether surface warming/cooling happens nearly immediate or with a delay when energy input from radiation changes. The steeper the slope, the faster the surface warming and the subsequent release of heat. The shallower the slope is, the slower and inefficient is this process. Slope and enclosed loop area are two independent properties. In order to assess the effect of a surface type on the heat storage contribution to UHI we need to consider both properties which is the reason why in Fig. 3 different clusters appear. The loops in Figs. S3 and S5 have different slopes and enclosed area sizes indicating a strong impact of the considered surface type, likewise. Surface types with similar properties in heat conductivity and heat capacity develop similar entropy loop characteristics. In that way, we can use the entropy loop framework as a generalization without knowing the exact thermal properties of a given surface. Entropy might be an indicator for assessing the effectivity of climate adaptation measures at locations with significant heat storage contributions to local UHI.

This is a new perspective on the heat storage related hysteresis: it might be an alternative to the original OHM formulation for urban heat storage change (*Oke et al., 2017*), and does not require regression coefficients for each surface type, individually. Especially in case of comprehensive urban planning processes our approach can support appropriate adaptation measures. Following the OHM parameterization after *Sun et al., 2017*, the entropy metric involves the heat conduction processes within the soil and their feedback to the surface level.

With heat conduction processes not only the amount but also the quality of energy and the change in quality (entropy) play an important role (*Herwig & Redecker, 2015*), because the change in energy quality indicates how efficiently heat is stored and released from the ground according to the used land surface type. Its thermal properties determine the amount of heat accumulation during heat episodes and the resulting proportion in the UHI intensity. An exact prediction of such a daily loop behaviour requires knowledge about how radiation energy is distributed among the surface energy balance terms. Since we are only interested in the state at a specific time, entropy helps to simplify the loop prediction because with this metric it does not matter how this state was achieved.

It should be noted that we neglected dissipated thermal energy in eq. 1. The ellipse for $\Delta S_{t,model}$ is an idealised solution of eq. 1 for a semi – infinite medium which might not perfectly fit to the boundary conditions of ENVI-met. A complete description of the energy exchange between soil/surface and the urban atmosphere would involve all surface energy balance terms. Since the surface UHI (ΔT) depends not only on the change in heat storage but rather on all biophysical contributions (radiation, evapotranspiration, convection, …), the hysteresis loop is a result of the amount of energy which is taken from the radiation. Therefore it is recommendable to extend the entropy perspective to all these processes. In this study, liquid water transport within soil was neglected since the standard volumetric water content for ENVI-met soils (see 3.1) is very low except for the high vegetation types. Nevertheless, soil wetness can affect the hysteresis loop orientation (*Sun et al., 2013*) and heat conduction (*Sun et al., 2017*). Future entropy related works should account for this.

5 CONCLUSION

An important strength of the suggested entropy framework is the site-independency enabling easy transferability to other urban locations and cities worldwide. In case that heat fluxes and surface temperatures (Q_t and $T_{t,sfc}$) are known, either from measurements or simulations, our approach is not limited by, e.g., the geology or geographical location of an area of interest. The conclusions for entropy optimization depend only on the soil/surface materials. Since entropy is a state variable, additional information, such as the depth of heat conduction, is contained in this quantity and not required for each location and time of the day. Our framework is model driven, which allows for a coverage of larger areas (and not restricted to pure point measurements) and makes it site-independent. Typically, in the urban context, gathering temperature and ground heat flux data is difficult and not comparable between different sites.

We emphasize that our results have some crucial implications for targeted local heat adaptation measures as follows:

(1) The hysteresis loop between heat storage (ground heat flux) and net radiation can be explained by the daily cycle of a thermodynamic state variable, a so-called entropy loop. This allows for an interpretation of the enclosed loop area as a measure of the consumed amount of radiation energy as well as the effectiveness of heat storage and release throughout the day. The slope of the entropy loop characterises the phase shift which determines how fast surface warming or cooling takes place. (Table 1)

(2) The entropy loop can be estimated with a heat conduction model to which the enclosed loop area is in good agreement (eqs. 4 - 6).

(3) From the entropy loop properties it can be concluded that, for the mitigation of heat episodes (exemplified for 11:00 at September 23rd, 2010, Fig. 3), the enclosed loop area should be maximised and that the curve should follow a symmetrical ellipse (Fig. 2), balancing heat storage and release. In addition, the slope of the entropy ellipse should be steep in order to enhance heat transport into ground and favour faster surface cooling relative to the rural situation. Only the combination of both properties helps to assess which surface type is superior with respect to climate adaptation.

For urban heat management, practitioners could use our approach together with Fig. 3 for an assessment of the feasibility of adaptation measures related to heat storage. We demonstrated that the daily heat storage cycle splits up into a temporal (slope) and spatial (energy amount – enclosed loop area) property. Especially, the temporal dynamic is an important criterion given by our entropy approach. For instance, sand has a large slope but high vegetation, such as trees or hedges, have a much shallower slope, although the enclosed loop area is similar for both (Fig. 3). While the sand surface heats up during day and cools down very fast during night, vegetation shows a delay influencing day and night temperatures differently. As a consequence it is insufficient to simply assess whether an adaptation measure has a warming or cooling effect (see ΔT_{stor} in Fig. 3). It is important at which time and location during the day which effect occurs. Therefore, we highly recommend that practitioners not only consider spatial temperature characteristics but also incorporate the temperature dynamics via our combined 'enclosed loop area – slope' approach. If one analyses Fig. 3 for each hour of the day it helps to find suitable surface covers mitigating heat accumulation. Without the two properties from our entropy ellipsis, it seems impossible to select suitable surface types. For example, sand and vegetation have a similar ΔT_{stor} at noon (around 0, Fig. 3), they only differ in their slopes. Marble pavements (not considered in Fig. 3) we could expect to be placed at the top right corner of Fig. 3, far above sand, since the heat capacity (indirect measure for the enclosed loop area) is similar than asphalt but the heat conductivity (indirect measure for the temporal dynamics and, thus, slope) is 4 times larger. For climate adaptation, surface types within cities should be as close as possible to the top right corner of Fig. 3, because they can store a large amount of heat (and provide cooling during daytime) but, after sunset, can release it very quickly, avoiding heat accumulation during night. In combination with other aspects (e.g. costs, irrigation availability, exposure to sun radiation…), the properties of the site-specific entropy loops can help to decide which surface types have the greatest mitigation effect. A possible workflow for an arbitrary location would involve first, micrometeorological simulations with the planned adaptation measures (e.g. different surface materials), second, application of our suggested entropy analysis, third, deriving evaluation graphs such as Fig. 3. If only a specific point is of interest and measurements for surface temperature and ground heat flux are available, the simulation part can be skipped.

Technical solutions for urban heat adaptation in future planning processes should pay more attention to the mitigation of individual UHI contributions. Ideally, urban surfaces should counteract dominant UHI contributions at the respective location by balancing optimised heat storage entropy, enhanced convection efficiency, and allowing for evapotranspiration (permeable/semi-permeable surfaces, porous asphalt materials (*Stempihar et al., 2012*) or green streets (*Im, 2019*)). Such a comprehensive analysis is urgently needed. Note that cement concrete has a lower heat island potential than porous asphalt (*Yang et al., 2020*). Here, only the heat storage effect was considered but not the evapotranspiration, which does not give the total benefit for urban heat reduction. Therefore we strongly recommend a consideration of all UHI contributions for heat management in future urban planning.

Acknowledgments

D.H. is funded by the Helmholtz-Climate-Initiative. The Helmholtz-Climate-Initiative (HI-CAM) is funded by the Helmholtz Associations Initiative and Networking Fund. The authors are responsible for the content of this publication.

REFERENCES

Brunsell, N.A.; Schymanski, S.J.; Kleidon, A. Quantifying the thermodynamic entropy budget of the land surface: is this useful? *Earth Syst. Dynam.* **2011**, *2*, 87-103; https://doi.org/10.5194/esd-2-87-2011

Bruse, M.; Fleer, H. Simulating surface-plant-air interactions inside urban environments with a three dimensional numerical model. *Environ. Model. Software* **1998**, *13*, 373-384; https://doi.org/10.1016/S1364-8152(98)00042-5

Camuffo, D.; Bernardi, A. An observational study of heat fluxes and their relationships with net radiation. *Bound.-Lay. Meteorol.* **1982**, *23*, 359-368; https://doi.org/10.1007/BF00121121

Capozzoli, A., Gorrino, A., Corrado, V. Thermal Characterization of Green Roofs through Dynamic Simulation. In *Proceedings of BS2013:* 13th Conference of International Building Performance Simulation Association, Chambéry, France, August 26-28; Wurtz, E., Ed.; IBPSA, Eindhoven, 2013; pp 3505–3512

Christidis, N.; Jones, G.S.; Stott, P.A. Dramatically increasing chance of extremely hot summers since the 2003 European Heatwave. *Nat. Clim. Change* **2015**, *5*, 46-50; https://doi.org/10.1038/NCLIMATE2468

Clausius, R. Ueber verschiedene für die Anwendung bequeme Formen der Hauptgleichungen der mechanischen Wärmetheorie. *Ann. Phys.* **1865**, *201*, 353-400; https://doi.org/10.1002/andp.18652010702

Creutzig, F.; Lohrey, S.; Bai, X.; Baklanov, A.; Dawson, R.; Dhakal, S.; Walsh, B.

Upscaling urban data science for global climate solutions. *Global Sustainability* **2019**, 2, E2. https://doi.org/10.1017/sus.2018.16

Forsythe, G.E.; Malcolm, M.A.; Moler, C.B. *Computer Methods for Mathematical Computations*; Englewood Cliffs Prentice Hall: Englewood Cliffs, N.J., 1977.

H.G. Fortak. Entropy and Climate. *Dev. Atmosph.* **10**, 1 – 14 (1979). https://doi.org/10.1016/B978-0-444-41766-4.50008-4

Grimmond, C.S.B.; Cleugh, H.A.; Oke, T.R. An objective urban heat storage model and its comparison with other schemes. *Atmos. Environ.* **1991**, *25* (3), 311-326; https://doi.org/10.1016/0957-1272(91)90003-W

Hamdhan, I.N., Clarke, B.G. Determination of Thermal Conductivity of Coarse and Fine Sand Soils. In *Proceedings of WGC 2010*: Bali, Indonesia, 25–29 April, 2010.

Hertel, D.; Schlink, U. Decomposition of urban temperatures for targeted climate change adaptation. *Environ. Modell. Softw.* **2019a**, *113*, 20-28; https://doi.org/10.1016/j.envsoft.2018.11.015

Hertel, D.; Schlink, U. How to convert urban energy balance into contributions to urban excess temperatures? *MethodsX* **2019b**, *6*, 132-142; https://doi.org/10.1016/j.mex.2018.12.015

H. Herwig, C. Redecker. “Heat Transfer and Entropy” in *Heat Transfer Studies and Applications*, S.N. Kazi, Ed. (Intech Open Limited, London, 2015). https://doi.org/10.5772/60610

Im, J. Green Streets to Serve Urban Sustainability: Benefits and Typology. *Sustainability*

2019, *11*, 6483; https://doi.org/10.3390/su11226483

Kalnay, E.; Cai, M. Impact of urbanization and land-use change on climate. *Nature* **2003** 423, 528–531. https://doi.org/10.1038/nature01675

Kuttler, W., Climate change on the urban scale – effects and countermeasures in Central Europe. In: *Human and Social Dimensions of Climate Change*; Chhetri, N., Ed.; IntechOpen Limited: London 2012, ch. 6, pp. 105-142; http://dx.doi.org/10.5772/50867

Kuricheva, O.; Mamkin, V.; Sandlersky, R.; Puzachenko, J.; Varlagin, A.; Kurbatova, J. Radiative Entropy Production along the Paludification Gradient in the Southern Taiga. *Entropy* **2017**, *19* (1), 43; https://doi.org/10.3390/e19010043

Lettau, H. Theory of surface-temperature and heat-transfer oscillations near a level ground surface. *Eos Trans AGU* **1951**, *32* (2), 189-200; https://doi.org/10.1029/TR032i002p00189

Li, D.; Liao, W.; Ridgen, A.J.; Liu, X.; Wang, D.; Malyshev, S.; Shevliakova, E. Urban heat island: Aerodynamics or imperviousness? *Sci. Adv.* **2019**, *5* (4); https://dx.doi.org/10.1126/sciadv.aau4299

Liu, C.; Liu, Y. Negative entropy flow and its effect on the organization of synoptic-scale severe atmospheric systems. *Geophys. Res. Lett.* **2004**, *31*, L01108; https://doi.org/10.1029/2003GL018071

Morabito, M.; Crisci, A.; Messeri, A.; Messeri, G.; Betti, G.; Orlandini, S.; Raschi, A.; Maracchi, G. Increasing heatwave hazards in the southeastern European Union capitals. *Atmosphere* **2017**, *8*; https://doi.org/10.3390/atmos8070115

Oh, J.W.; Ngarambe, J.; Duhirwe, P.N.; Yun, G.Y. Using deep-learning to forecast the magnitude and characteristics of urban heat island in Seoul Korea. Sci. Rep. **2020**, 10, 3559. https://doi.org/10.1038/s41598-020-60632-z

Oke, T.R. City size and urban heat island. *Atmos. Environ.* **1973**, 7, 769-779. https://doi.org/10.1016/0004-6981(73)90140-6

Oke, T.R.; G. Mills, A. Christen, J.A. Voogt, "Heat Storage Change" in *Urban Climates* (Cambridge University Press, 2017), pp. 168–175.

Purvis, B.; Mao, Y.; Robinson, D. Entropy and its application to urban systems. *Entropy* **2019**, *21* (1), 56; http://dx.doi.org/10.3390/e21010056

Ridgen, A.J.; Li, D. Attribution of surface temperature anomalies induced by land use and land cover changes. *Geophys. Res. Lett.* **2017**, *44*, 6814-6822; https://doi.org/10.1002/2017GL073811

Roxy, M.S.; Sumithranand, V.B.; Renuka, G. Estimation of soil moisture and its effect on soil thermal characteristics at Astronomical Observatory Thiruvananthapuram, south Kerala. *J Earth Syst. Sci.* **2014**, *123*, 1793–1807; https://doi.org/10.1007/s12040-014-0509-x

Schlink, U.; Kindler, A.; Großmann, K.; Schwarz, N.; Franck, U. The temperature recorded by simulated mobile receptors is an indicator for the thermal exposure of the urban inhabitants. *Ecol. Indic.* **2014**, *36*, 607-616; https://doi.org/10.1016/j.ecolind.2013.09.017

Singh, V.P. Entropy theory for movement of moisture in soils. *Water Resour. Res.* **2010**, *46*, W03516; https://dx.doi.org/10.1029/2009WR008288

Stempihar, J.J.; Pourshams-Manzouri, T.; Kaloush, K.E.; Rodezno, M.C. Porous Asphalt Pavement Temperature Effects for Urban Heat Island Analysis. *Transp Res Record* **2012**, *2293*(1), 123-130; https://doi.org/10.3141/2293-15

Sun, T.; Wang, Z.-H.; Ni, G.-H. Revisiting the hysteresis effect in surface energy budgets. *Geophys. Res. Lett.* **2013**, *40*, 1741 – 1747; https://doi.org/10.1002/grl.50385

Sun, T.; Wang, Z.-H.; Oechel, W.C.; Grimmond, S. The Analytical Objective Hysteresis Model (AnOHM v1.0): methodology to determine bulk storage heat flux coefficients. Geosci. Model Dev. **2017**, *10*, 2875 – 2890; https://doi.org/10.5194/gmd-10-2875-2017

U.S. Department of Transportation – Federal Highway Administration Home Page. https://www.fhwa.dot.gov/pavement/sustainability/articles/pavement_thermal.cfm (last access, Nov 27, 2020)

W. Wu, Liu. Radiation entropy flux and entropy production of the Earth system. *Rev. Geophys.* **48**, 2 (2010). https://doi.org/10.1029/2008RG000275

World Urban Database and Access Portal Tools – WUDAPT Home Page. https://www.wudapt.org/ (last access, Apr 21, 2021)

Yang, H.; Yang, K.; Miao, Y.; Wang, L.; Ye, C. Comparison of Potential Contribution of Typical Pavement Materials to Heat Island Effect. *Sustainability* **2020**, *12*, 4752; https://doi.org/10.3390/su12114752

Zednik, C. Solving the Black Box Problem: A Normative Framework for Explainable Artificial Intelligence. Philos. Technol. **2019**. https://doi.org/10.1007/s13347-019-00382-7

Zhao, L.; Lee, X.; Smith, R.B.; Oleson, K. Strong contributions of local background climate to urban heat islands. Nature **2014**, 511, 216-219; https://doi.org/10.1038/nature13462

Supplementary Material for

Entropy frameworks for urban heat storage can support targeted adaptation strategies

Daniel Hertel, Uwe Schlink*

Helmholtz Centre for Environmental Research – UFZ, Department of Urban and Environmental Sociology, Permoserstraße 15, 04318, Leipzig, Germany

<u>Content:</u>

12 Pages

2 Tables

6 Figures

*Corresponding Author

Phone: + 49 341 235 1704

Fax: +49 341 235 45 1704

E-mail: daniel.hertel@ufz.de

Location of the surface types in ENVI-met (area input file)

Figure S1. Location of the various surface types within the simulation area. Above: Built-up structure; green denotes all surface types with vegetation (LAD means 'leaf area density'). The lowest LAD represents "loam with grass" and the highest 'loam with hedge'. Below: brown is loamy soil, light yellow is sand, grey is concrete pavement, orange is brick-red, dark yellow is brick-yellow and black is asphalt.

Table S1. Configuration settings of ENVI-met.

Variable	Value
start simulation (day, time)	22.09.2010, 00:00:00
total simulation time	48 h; only 2nd day was used for analysis
save model state	each 60 min
wind speed (10 m above ground) [m/s]	1.7
wind direction [°]	103
roughness length at reference point	0.1
temperature atmosphere [K]	daily profile
specific humidity in 2500 m [g/kg]	1.2
relative humidity in 2 m [%]	daily profile

Table S2. Surface types as used in ENVI-met and their respective surface areas.

Surface Type	Area Size [m²]
asphalt	41715
sand	6678
brick-yellow	1638
brick-red	14382
concrete pavement	2556
loam	287199
bare soil	143262
loam with grass	78939
loam with tree (10 m, LAD: 2.18)	6273
loam with tree (15 m), LAD: 1.15)	22356
loam with hedge	6075

Validation of simulated surface temperatures

The mostly negative differences between the observed thermal image and ENVI-met simulations ($T_{simulated}$ - $T_{observed}$) indicate that ENVI-met underestimates the surface temperature in most areas of the neighbourhood (Fig. S2). Highest negative values can be found next to the periphery of the buildings and preferably inside courtyards. Positive values (overestimation) are associated with streets (asphalt) and concrete (pavement) surfaces.

The total range of values is between -11 K and +5 K (two-third is in the range of -5 K and +2 K) and tend to be negative (underestimation). This is in accordance with findings from other studies utilizing ENVI-met simulations. For instance, for air temperatures during the day in Sao Paolo, *Gusson & Duarte (2016)* found an underestimation of around 3 K.

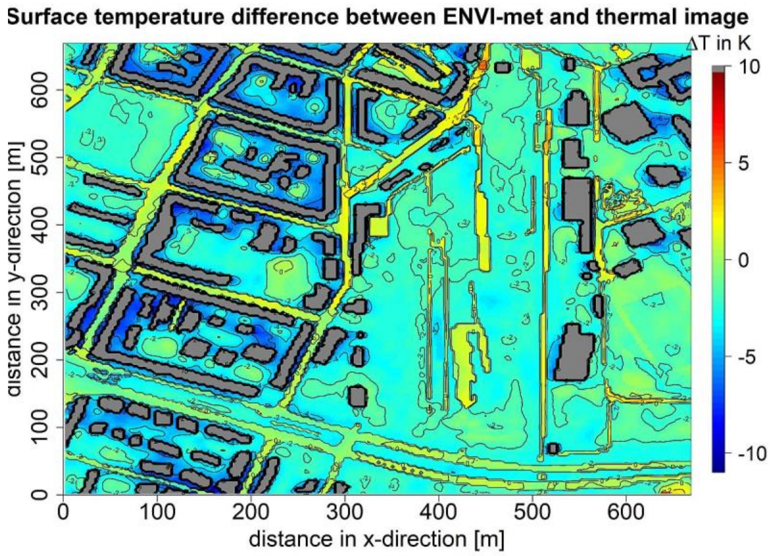

Figure S2. Difference between ENVI-met simulation and thermal image for 'Bayerischer Bahnhof' area in Kelvin [K]. Negative values denote that ENVI-met underestimates the surface temperature.

Heat conduction model

Introducing dimensionless variables by characteristic quantities (denoted with a ~) such as length (x*), time (t*) and temperature (u*)

$$x^{\sim} = \frac{x}{x^*}; \quad t^{\sim} = \frac{t}{t^*}; \quad u^{\sim}(x^{\sim}, t^{\sim}) = \frac{u(x,t)}{u^*} \tag{S1}$$

in eq. 3 of the main text yields,

$$\frac{\partial u^{\sim}}{\partial t^{\sim}} = \frac{t^* D}{x^{*2}} \frac{\partial^2 u^{\sim}}{\partial x^{\sim 2}}. \tag{S2}$$

The characteristic dimension of $t^*$is one day (t_{24}) and $u^* = T_0$.

For the characteristic time we set $t^* = \frac{x^{*2}}{D}$, select x^*so that $\frac{t^* D}{x^{*2}} = 1 \rightarrow x^* = \sqrt{t^* D}$ and ignore the ~ notation, which simplifies eq. 3 in the main text to

$$\frac{\partial u(x,t)}{\partial t} - \frac{\partial^2 u(x,t)}{\partial x^2} = 0; \quad x > 0; \quad t > 0. \tag{S3}$$

For the decay condition a quasi-steady state $\left(\frac{\partial u}{\partial t} = 0\right)$ solution satisfies the given problem. The generalised solution is superposed by 2 individual solutions:

$u(x,t) = u_0 + u_1.$

For u_0, the boundary condition (BC; see chapter 2.3 in main text) becomes $u_0(0,t) = T_0$. The resulting solution is $u_0(x,t) = T_0$, which is the only one because of the uniqueness criterion. For u_1 (BC becomes $u_1(0,t) = -T_1 \cos(\omega t)$) we assume an amplitude C(x) and a phase shift $\phi(x)$ depending on the soil depth x

$$C(x) \cos\big(\omega t - \phi(x)\big) = Re\big\{C(x) e^{-i\phi(x)} e^{i\omega t}\big\} = Re\big\{U(x) e^{i\omega t}\big\}. \tag{S4}$$

Inserting eq. S4 into eq. S3, by using the relation $Re\big\{U(x)e^{i\omega t}\big\} = 1/2\big\{U(x)e^{i\omega t} + U^{\#}(x)e^{-i\omega t}\big\}$ with # denoting the complex conjugate, gives

$$\frac{1}{2}\left(i\omega U(x)e^{i\omega t} - i\omega U^{\#}(x)e^{-i\omega t}\right) = \frac{1}{2}\left(U''(x)e^{i\omega t} + U''^{\#}(x)e^{-i\omega t}\right). \tag{S5}$$

Reformulation yields

$$\Bigg(\underbrace{i\omega U(x) - U''(x)}_{a}\Bigg)e^{i\omega t} + \Bigg(\underbrace{-i\omega U^{\#}(x) - U''^{\#}(x)}_{b}\Bigg)e^{-i\omega t} = 0. \tag{S6}$$

With a=b=0 and inserting the BC into eq S5, it follows

$$U''(x) - i\omega U(x) = 0,\ x > 0 \tag{S7}$$

$$U(0) = -T_1,\ U\ is\ bounded\ for\ x \to \infty,\ t > 0.$$

Now, eq. S7 represents an ordinary differential equation (ODE) which is easier to solve than the partial differential equation (PDE) in eq. S3. It can be solved in order to obtain a solution for u_1.

With $i\omega = \frac{1}{2}(1+i)^2\omega = \left(\sqrt{\frac{\omega}{2}}(1+i)\right)^2$, the general solution for eq. S7 has the form

$$U(x) = C_1 e^{-\sqrt{\frac{\omega}{2}}(1+i)x} + C_2 e^{\sqrt{\frac{\omega}{2}}(1+i)x}. \tag{S8}$$

The constants C_1 and C_2 need to be determined by help of the BCs. In case of x → ∞, $e^{-\sqrt{\frac{\omega}{2}}(1+i)x} \to 0$ and $e^{\sqrt{\frac{\omega}{2}}(1+i)x} \to \infty$ which gives $C_2 = 0$ as the only solution. For U(0) it follows, $U(0) = C_1 + C_2 = -T_1$ and hence $C_1 = -T_1$. Thus, eq. S8 simplifies to

$$U(x) = -T_1 e^{\left(-\sqrt{\frac{\omega}{2}}(1+i)x\right)}. \tag{S9}$$

Eq. S9 is the complex solution of u_1. Combining u_0, u_1 and make use of relation S4 it yields

$$u(x,t) = T_0 + Re\left\{-T_1 e^{-\sqrt{\frac{\omega}{2}}(1+i)x} e^{i\omega t}\right\}. \tag{S10}$$

A reformulation gives

$$\begin{aligned} u(x,t) &= T_0 - T_1 e^{-\sqrt{\frac{\omega}{2}}x} Re\left\{e^{-i\sqrt{\frac{\omega}{2}}x + i\omega t}\right\} \\ &= T_0 - T_1 e^{-\sqrt{\frac{\omega}{2}}x} \cos\left(-\sqrt{\frac{\omega}{2}}x + \omega t\right). \end{aligned} \tag{S11}$$

$\sqrt{\frac{\omega}{2}}x$ represents the phase $\phi(x)$ in eq. S4. Since we are looking for the surface, the soil depth x is 0 and the phase vanish. According to eq. S1, u is dimensionless which requires a retransformation of the parameter ω, t and x or in dimensionless notation ω~, t~ and x~. From relation S1 and the transition between eqs. S2 and S3 it follows

$$t^{\sim} = \frac{t}{t^*} = \frac{t}{\frac{x^{*2}}{D}} = t\,\frac{D}{x^{*2}}\,. \quad \text{(S12)}$$

D varies according to the respective soil material but here we assumed an effective value of $2 \times 10^{-3}\,\frac{cm^2}{s}$ as mean value (*Nakshabandi & Kohnke, 1964; Marquez et al., 2016*) for all surface types since deeper soil layers are the same (sand/loam). t is varied between 0 and 24 in steps of 1 h and multiplied by 3600 to convert hours into seconds. ω (ω~) can be calculated with

$$\tau = \frac{2\pi}{\omega} = t^{\sim}$$

$$\omega = \omega^{\sim} = \frac{2\pi}{t^{\sim}} = \frac{2\pi}{t^*\frac{D}{x^{*2}}}\,, \quad \text{(S13)}$$

with t* = 24 × 3600.

Inserting eqs. S12 – S13 into eq. S11 we obtain

$$u(x,t) = T_0 - T_1 e^{-\sqrt{\frac{\frac{2\pi}{t^*\frac{D}{x^{*2}}}}{2}}\frac{x}{x^*}} \cos\left(-\sqrt{\frac{\frac{2\pi}{t^*\frac{D}{x^{*2}}}}{2}}\,\frac{x}{x^*} + \frac{2\pi}{t^*\frac{D}{x^{*2}}}\,t\,\frac{D}{x^{*2}}\right). \quad \text{(S14)}$$

After differentiating eq. S14 with respect to x and multiplying the thermal conductivity λ we gain the continuous ground heat flux Q(t)

$$Q(t) = -\lambda \frac{\partial u(x,t)}{\partial x}\ \Big|_{x=0}$$

$$= -\lambda \times T_1 \frac{1}{x^*}\sqrt{\frac{\frac{2\pi}{t^*\frac{D}{x^{*2}}}}{2}}\, e^{-\sqrt{\frac{\frac{2\pi}{t^*\frac{D}{x^{*2}}}}{2}}\frac{x}{x^*}} \left(\cos\left(\left(-\sqrt{\frac{\frac{2\pi}{t^*\frac{D}{x^{*2}}}}{2}}\,\frac{x}{x^*} + \frac{2\pi}{t^*\frac{D}{x^{*2}}}\,t\,\frac{D}{x^{*2}}\right) - \psi\right) - \right.$$

$$\left. \sin\left(\left(-\sqrt{\frac{\frac{2\pi}{t^*\frac{D}{x^{*2}}}}{2}}\,\frac{x}{x^*} + \frac{2\pi}{t^*\frac{D}{x^{*2}}}\,t\,\frac{D}{x^{*2}}\right) - \psi\right)\right). \quad \text{(S15)}$$

Daily cycles of Q_t and u(x=0, t) are delayed against each other (*Lettau, 1951*) so that we have to add the phase shift ψ and estimate it during the fitting procedure.

Entropy loops for all surface types

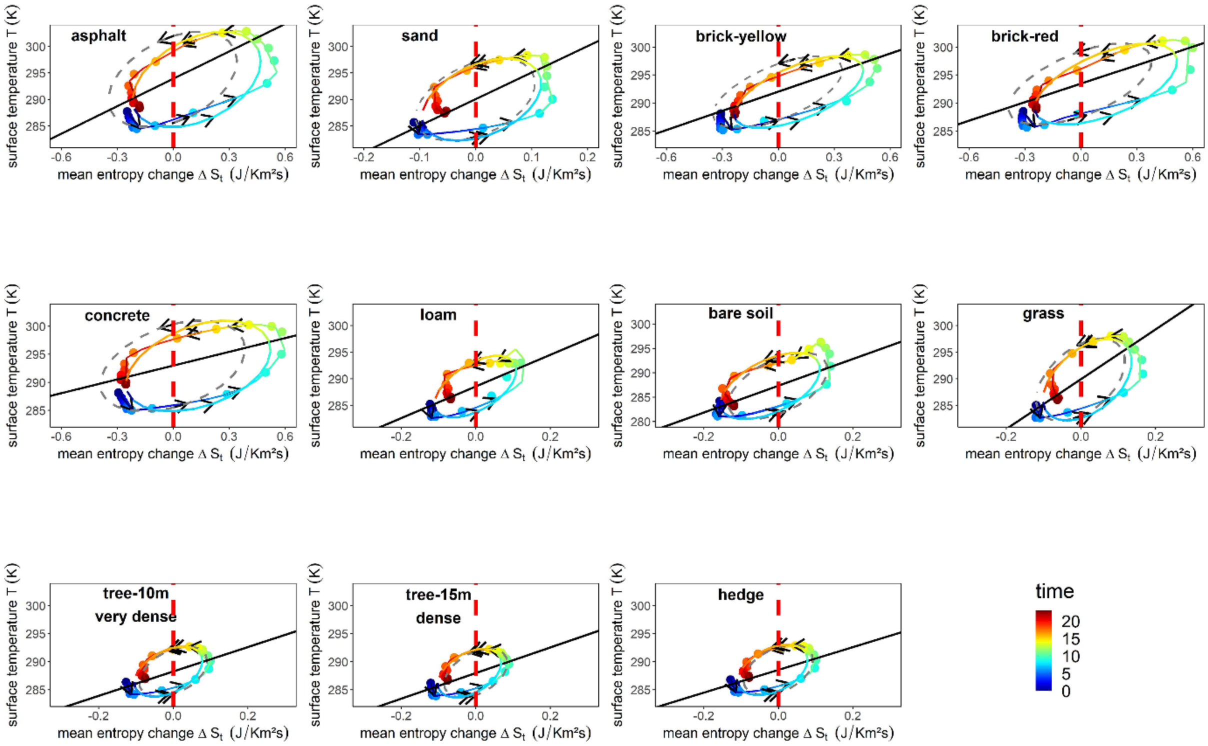

Figure S3. Change in entropy (J/Km²) at time t (current hour) versus current mean surface temperature for all defined surface types. The ellipses represent a fitted ideal heat conduction model (grey dashed without adding an additional heat flux; thick coloured line with adding a heat flux), the thin coloured line shows eq. 2 (main text) fitted with a cubic smoothing spline. Original plot for eq. 2 (main text) are the coloured points around the spline. All Figures were made for September 23rd commencing at 0:00; colours represent time. Arrows denote the looping direction. The red dashed vertical line (ΔS_t = 0) separates between upward and downward change in entropy. The diagonal black line is a linear regression line indicating the slope of the ΔS_t loop.

Daily cycles of the surface temperature and hourly temperature gradient for all surface types

The simulated surface temperature has no sharp peak but rather a kind of a plateau. This becomes obvious by analysing the temporal gradient for each hour (red lines in Figure S3), especially for the “loam with tree” surface types.

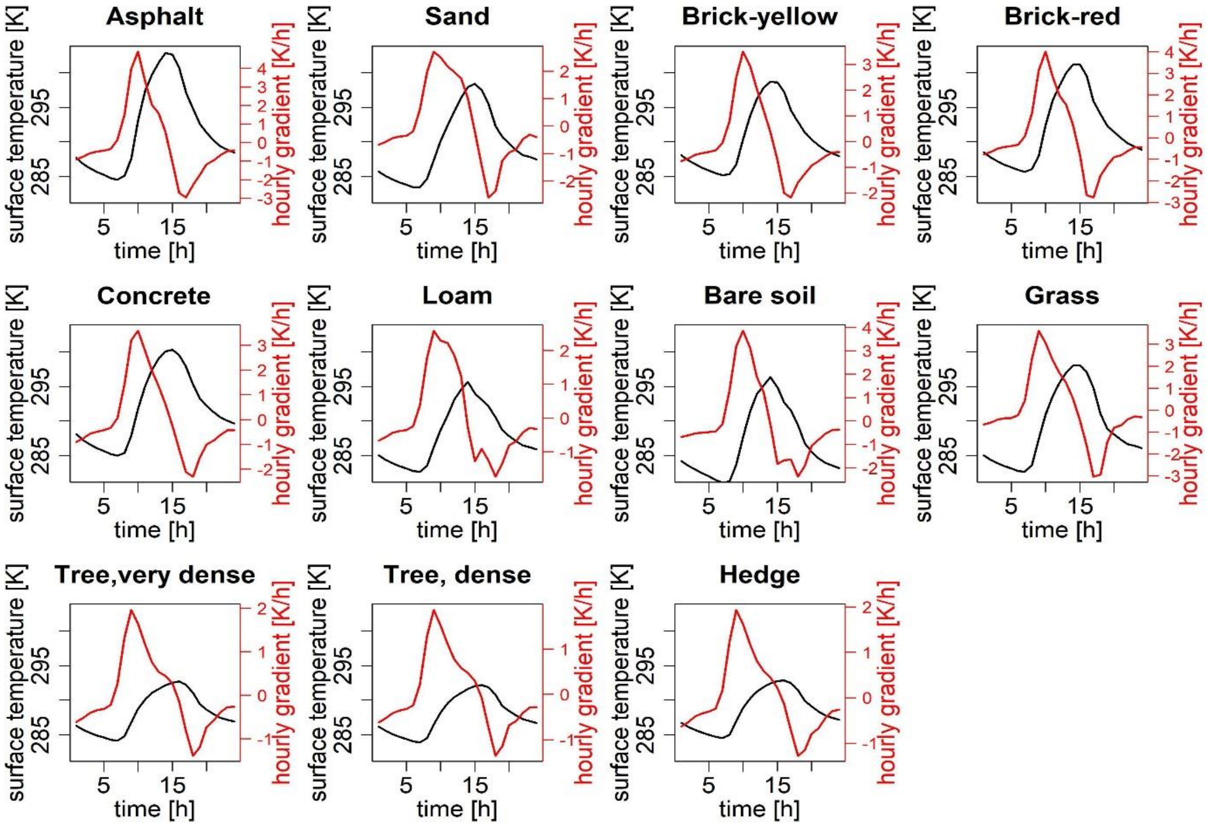

Figure S4. Mean surface temperature in Kelvin (black line) and approx. gradient (red line) for all defined surface types (order is same as Figure S2) dependent on hour of the day (23 September 2010, commencing at 0:00).

The gradient per hour denotes the magnitude and direction of ground heat flux. The stronger the gradient the stronger the ground heat flux. The surface temperature peaks when the gradient is 0. After the minimum of the gradient curve (red line in Figure S3) is passed through, ground heat flux becomes negative (changes direction) and slows down during night since the temperature gradient is near 0. At 10:00 the increase of the surface temperature starts to reduce which is why the gradient curve shows a small bulge. Right after the beginning of this process, at 11:00, the ground heat flux reaches its maximum while the surface temperature increases further until 13:00. This influences the slope and the enclosed area of the entropy loop. Without delay the slope would be much steeper and the enclosed area smaller.

Relation between ground heat flux and change in entropy

Considering the entropy loop as a thermodynamic cycle (T-S diagram) for a soil system then a change in surface temperature triggers a ground heat flux that, in turn, changes the state variable entropy. If we ignore the system state and analyse the ground heat flux only as a function of surface temperature (Figure S3), resulting Q-T diagram is a direct consequence out of the change in the system state (entropy loop; see Figure 2 in main text). Thus, it describes a hysteresis similar to Grimmond's proposal *(Grimmond et al., 1991*). Q and S are coupled with eq. 2 (main text) where the entropy can only be negative if the ground heat flux for a given hour is negative, which means that the transfer is directed into the atmosphere (positive means that it is directed into the ground).

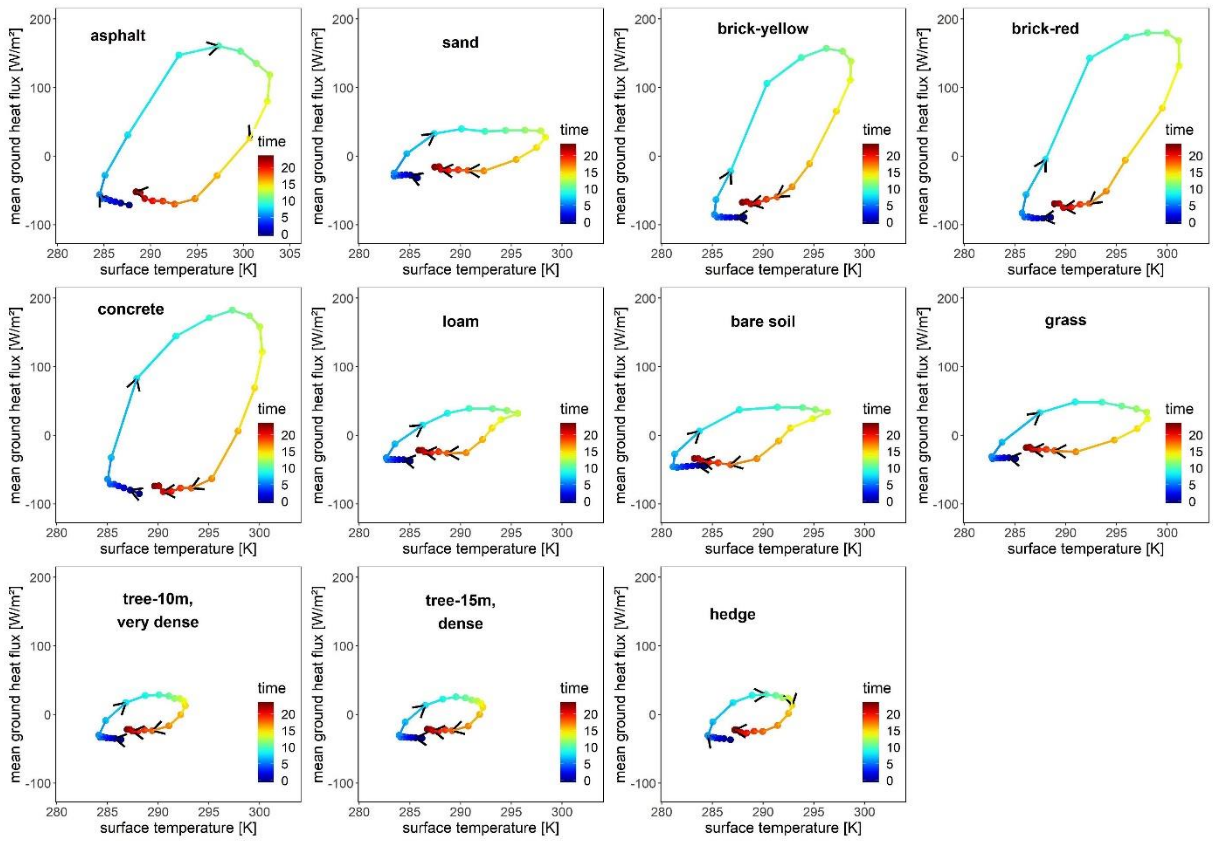

Figure S5. Ground heat flux (W/m²) vs. surface temperature (K) for all defined surface types. Colours denote hour of the day (23 September 2010, starting at 0:00). Arrows denote looping direction.

The advantage of a Q-T rather than a Q-R (ground heat flux vs. net radiation) diagram comes from the easier interpretation with an entropy loop since the ground heat flux directly depends on the surface temperature. For net radiation it is more difficult since not all of the energy is transformed into a ground heat flux. Rather it is distributed according to the surface energy balance terms as was stated in the UHI decomposition framework.

Hysteresis loops for all surface types

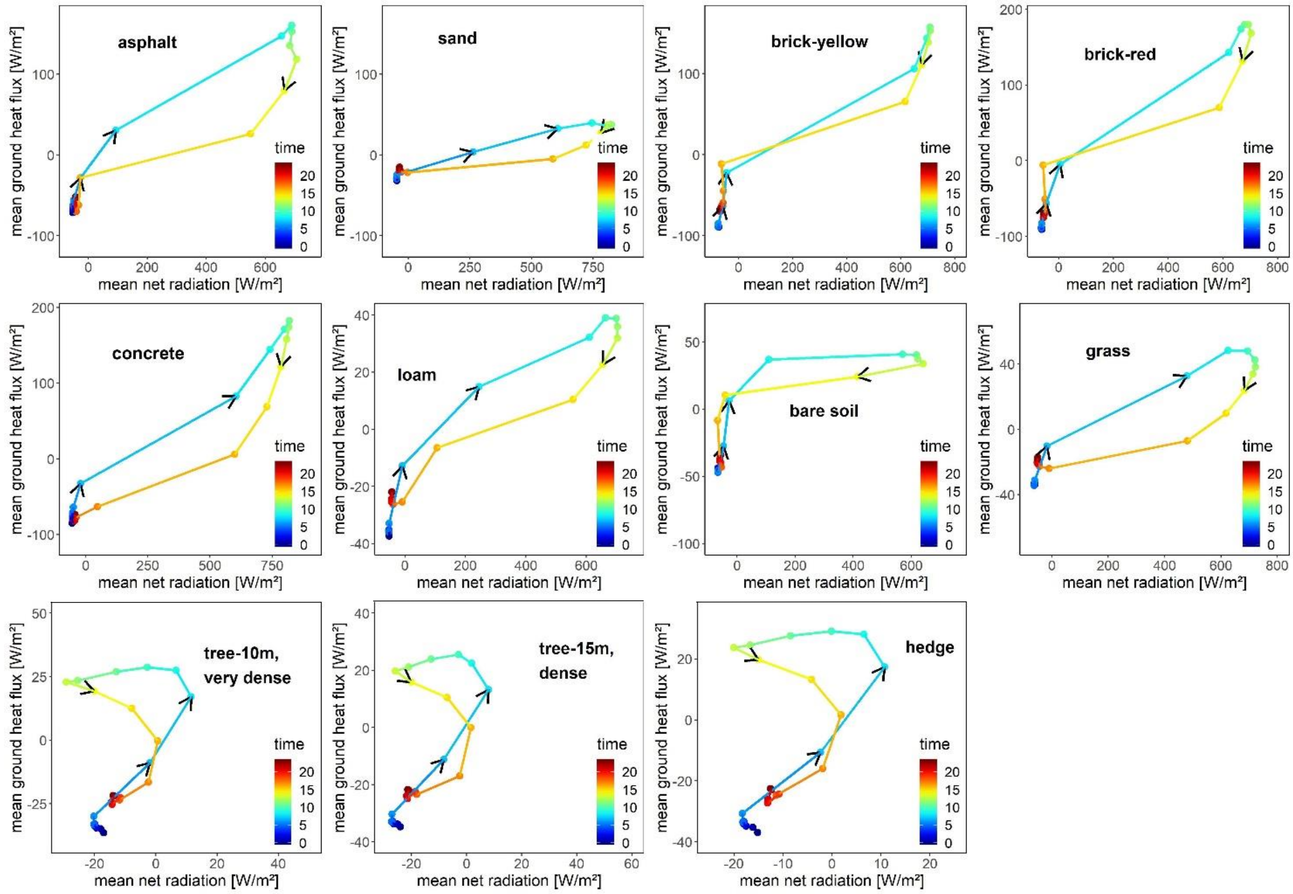

Figure S6. Mean ground heat flux [W/m²] vs. mean net radiation [W/m²] for all surface types (order is same as Figure S2) per hour of the day (coloured; 23 September 2010, commencing at 0:00 a.m.).

REFERENCES

Lettau, H. Theory of surface-temperature and heat-transfer oscillations near a level ground surface. *Eos Trans AGU* **1951**, *32* (2), 189-200; https://doi.org/10.1029/TR032i002p00189

Nakshabandi, G. Al; Kohnke, H. Thermal conductivity and diffusivity of soils as related to moisture tension and other physical properties. *Agr. Meteorol.* **1964**, *2*, 271-279; https://doi.org/10.1016/0002-1571(65)90013-0

Márquez, J.M.A.; Behórquez, M.A.M.; Melgar, S.G. Ground thermal diffusivity calculation by direct soil temperature measurement. Application to very low enthalpy geothermal energy systems. *Sensors* **2016**, *16* (3), 306; https://doi.org/10.3390/s16030306

Grimmond, C.S.B.; Cleugh, H.A.; Oke, T.R. An objective urban heat storage model and its comparison with other schemes. *Atmos. Environ.* **1991**, *25* (3), 311-326; https://doi.org/10.1016/0957-1272(91)90003-W

Gusson, C.S.; Duarte, D.H.S. Effects of built density and urban morphology on urban microclimate – calibration of the model ENVI-met V4 for the subtropical Sao Paolo, Brazil. *Procedia Engineering* **2016**, *169*, 2-10; https://doi.org/10.1016/j.proeng.2016.10.001